Article:
Stamatiou, IK orcid.org/0000-0002-3862-309X and Muller, FL orcid.org/0000-0002-8507-4193 (2017) Determination of mass transfer resistances of fast reactions in three-phase mechanically agitated slurry reactors. AIChE Journal, 63 (1). pp. 273-282. ISSN 0001-1541

https://doi.org/10.1002/aic.15540

AIChE Journal
DOI 10.1002/aic.15540

DETERMINATION OF MASS TRANSFER RESISTANCES OF FAST REACTIONS IN THREE-PHASE MECHANICALLY AGITATED SLURRY REACTORS

Ilias K. Stamatiou and Frans L. Muller

Institute of Process Research and Development (iPRD), University of Leeds,

Leeds, LS2 9JT, United Kingdom

Correspondence concerning this article should be addressed to I. K. Stamatiou at

pmist@leeds.ac.uk.

Introduction

Gas-liquid-solid three phase reactors are of great importance in pharmaceutical and fine chemical industry. The mechanically agitated slurry reactors are the most common type of three phase reactors which are used within these industries [1].

During the three-phase reactions a number of mass transfer processes need to take place before the surface catalytic reaction: a) gas-liquid mass transfer, b) liquid-solid mass transfer and c) the combined internal pore diffusion and the surface chemical reaction. Each of the mass transfer processes and the intrinsic reaction rate affect the overall process rate in different extent [1, 2]. The design of three phase reactors requires the determination of the mass transfer coefficients and the reaction rate constant. The determination of mass transfer coefficients becomes even more important when the reaction rate constant and external mass transfer is of comparable magnitude. This happens in the case of fast

doi: 10.1002/aic.15540

Received: Apr 14, 2016; Revised: Sep 26, 2016; Accepted: Oct 06, 2016

chemical reactions. In fast chemical reactions, even if intense mixing conditions take place, the external mass transfer processes are not faster than the surface chemical reaction.

Many researchers have used several methods to separate the effect of each of the mass transfer coefficients. Currently, there is not any established methodology for the separation of each of the mass transfer coefficients and the reaction rate constant a) under the reaction conditions, b) without changing the size of the catalyst, c) under conditions which do not allow to neglect any of the rate and d) without needing to use low substrate concentration. Many researchers have studied the hydrogenations of unsaturated organic compounds by varying the hydrogen partial pressure but they have not manipulated the overall mass transfer resistance against the square root of hydrogen concentration in gas-liquid interface, $C_{H_2,i}/MTR_{H_2}$ versus $C_{H_2,i}{}^{0.5}$ [3, 4]. Tiwari et al. [5] used the plot of $C_{H_2,i}/MTR_{H_2}$ versus $C_{H_2,i}$ to calculate the reaction rate constant of the surface reaction of 3,4-dimethoxyphenone, but they assumed negligible external mass transfer resistance in their model. Joshi et al. [6] used also the these kind of plots to calculate the reaction constants of homogeneously catalysed styrene hydrogenation. The gas-liquid mass transfer coefficient is usually determined using the dynamic physical absorption method[2, 3, 7, 8]. Cordova and Harriott [9], Gholap et al. [10] calculated gas-liquid mass transfer coefficient and the liquid-solid mass transfer coefficient by changing catalyst loading and using different size of catalyst particle under reaction conditions. The drawback of varying catalyst size is the requirement of shell type catalyst to ensure interparticle diffusion does not depend on catalyst size. Ruether and Puri [11] separated the reaction rate constant from the mass transfer resistances but they used a very low concentration of substrate to obtain a first order reaction rate with respect to substrate concentration. In this case the limiting reactant

is the substrate, something that occurs in industrial hydrogenators only during the end of the batch reaction.

The objective of this paper is to build a methodology for the separation of mass transfer effects in three phase processes in mechanically agitated hydrogenators under the reaction conditions by manipulating the agitation speed and the hydrogen pressure, instead of changing catalyst size. We apply the concept of mass transfer resistance adopting the consideration of Levenspiel [12] about heterogeneous reactions. Therefore, we assume that mass transfer processes and chemical reaction take place in series.

Theoretical Background

Mass transfer in Hydrogenation process

The overall process of the styrene hydrogenation consists of four steps which take place in series[1, 9, 13-16]:

1. Absorption of H_2 into g-l interface from bulk gas phase

$$\mathrm{MTR}_{\mathrm{H_2},1} = \mathrm{K_G} \cdot \alpha \cdot \mathrm{H_E} \cdot \left(\frac{\mathrm{P}_{\mathrm{H_2,G}}}{\mathrm{H_E}} - \frac{\mathrm{P}_{\mathrm{H_2,i}}}{\mathrm{H_E}}\right) \quad (1)$$

2. Diffusion of H_2 into liquid phase from g-l interface

$$\mathrm{MTR}_{\mathrm{H_2},2} = \mathrm{K_L} \cdot \alpha \cdot (\mathrm{C}_{\mathrm{H_2,i}} - \mathrm{C}_{\mathrm{H_2,L}}) \quad (2)$$

3. Diffusion of H_2 from liquid phase to particle external surface

$$\mathrm{MTR}_{\mathrm{H_2},3} = \mathrm{K_S} \cdot \alpha_\mathrm{S} \cdot \frac{\mathrm{W_c}}{\mathrm{V_L}} (\mathrm{C}_{\mathrm{H_2,L}} - \mathrm{C}_{\mathrm{H_2,S}}) \quad (3)$$

4. Diffusion of H_2 through particle pore structure and chemical reaction on catalyst surface, assuming 1st order reaction with respect to H_2

$$\mathrm{MTR}_{\mathrm{H_2},4} = \varepsilon \cdot \mathrm{k'_{obs}} \cdot \frac{\mathrm{W_c}}{\mathrm{V}_L} \cdot \mathrm{C}_{\mathrm{H_2,S}} \quad (4)$$

In the case of pure hydrogen or slightly soluble gases, it is unlikely the absorption of H_2 to be the limiting step. As a result it is neglected and the concentration of H_2 at the g-l interface is considered to be in equilibrium with the gas phase pressure of hydrogen based on the Henry's law [15, 17].

$$P_{H_2} = \mathrm{H_E} \cdot \mathrm{C}_{\mathrm{H_2,i}} \quad (5)$$

Under the range of pressure and temperature we used the Henry constant, $\mathrm{H_E}$, is calculated by the correlation which is described by equation 6 where $\mathrm{H_E}$ in Mpa, T in K and P_{H_2} in Pa[18].

$$Ln(\mathrm{H_E}) = 122.3 - \frac{4815.6}{T} - 17.5 \cdot Ln(T) + 1.4 \cdot 10^{-7} \cdot P_{H_2} \quad (6)$$

Considering that the process reaches steady state conditions fast, the four steps take place under the same rate. The overall rate is determined by the slowest step.

$$\mathrm{MTR}_{\mathrm{H_2},1} = \mathrm{MTR}_{\mathrm{H_2},2} = \mathrm{MTR}_{\mathrm{H_2},3} = \mathrm{MTR}_{\mathrm{H_2},4} = \mathrm{MTR}_{\mathrm{H_2}} \quad (7)$$

From equations 1-5 and 7, we conclude to the expression of the overall mass transfer rate,

$$\mathrm{MTR}_{\mathrm{H_2}} = \frac{1}{\frac{1}{\mathrm{K_L} \cdot \alpha} + \frac{1}{\mathrm{K_S} \cdot \alpha_S \cdot \frac{\mathrm{W_c}}{\mathrm{V_v}}} + \frac{1}{\varepsilon \cdot \mathrm{k'_{obs}} \cdot \frac{\mathrm{W_c}}{\mathrm{V_L}}}} \cdot \frac{\mathrm{P}_{\mathrm{H_2}}}{\mathrm{H_E}} \quad (8)$$

From equation 8 we realise that the three components at the denominator act as barriers to the MTR, the higher they are the slower the rate. In an analogy to the Ohm's law, the components of the denominator are called resistances. The denominator represents the

overall mass transfer resistance, $\Omega_{H_2,tot}$, on the hydrogenation process. Table 1 gives the definition of each of the resistances.

By manipulating appropriately equations 1-5 and 7, we conclude to the following expressions for $C_{H_2,i}$, $C_{H_2,L}$ and $C_{H_2,S}$,

$$C_{H_2,i} = MTR_{H_2} \cdot \left[\frac{1}{K_L \cdot \alpha} + \frac{1}{K_S \cdot \alpha_S \cdot \frac{W_c}{V_L}} + \frac{1}{\varepsilon \cdot k'_{obs} \cdot \frac{W_c}{V_L}} \right] \quad (9)$$

$$C_{H_2,L} = MTR_{H_2} \cdot \left[\frac{1}{K_S \cdot \alpha_S \cdot \frac{W_c}{V_{v\,L}}} + \frac{1}{\varepsilon \cdot k'_{obs} \cdot \frac{W_c}{V_L}} \right] \quad (10)$$

$$C_{H_2,S} = MTR_{H_2} \cdot \frac{1}{\varepsilon \cdot k'_{obs} \cdot \frac{W_c}{V_L}} \quad (11)$$

To express hydrogen concentration on the external catalyst surface, $C_{H_2,S}$, as a function of the hydrogen concentration in gas-liquid interface, $C_{H_2,i}$, we introduce the factor β. Factor β is defined as the ratio between $\Omega_{H_2,R}$ and $\Omega_{H_2,tot}$.

$$C_{H_2,S} = \beta \cdot C_{H_2,i} \quad (12)$$

$$\beta = \frac{\Omega_{H_2,R}}{\Omega_{H_2,tot}} \quad (13)$$

Kinetics of surface catalytic reaction

The surface catalytic reaction can be broken down into the elementary steps. Figure 1 and 2 illustrates the dissociative and molecular chemisorption onto catalyst surface, assuming that the substrate and hydrogen do not compete for the same catalyst site. Figure 3 illustrates the surface chemical reaction which is the rate determining step [12, 19, 20].

1. Dissociative and molecular chemisorption onto the catalyst surface

A) Hydrogen dissociative chemisorption[21-25]

At the equilibrium,

$$K_H = \frac{C_{H-M1}^2}{C_{H_{2,S}} \cdot C_{M1}^2} \Rightarrow C_{H-M1} = \sqrt{K_H \cdot C_{H_{2,S}}} \cdot C_{M1} \quad (14)$$

B) Molecular chemisorption of unsaturated organic compound

At the equilibrium,

$$K_R = \frac{C_P}{C_{R-CH=CH_{2,S}} \cdot C_{M2}^2} \Rightarrow C_P = K_R \cdot C_{R-CH=CH_{2,S}} \cdot C_{M2}^2 \quad (15)$$

2. Chemical reaction on catalyst surface and desorption of product from catalyst surface.

The rate of surface chemical reaction is,

$$-R'_{H_2} = \varepsilon \cdot k' \cdot C_P \cdot C_{H-M1}$$

Substituting the expressions of $H - M1$ and P,

$$-R'_{H_2} = \varepsilon \cdot k'_o \cdot C_{R-CH=CH_{2,S}} \cdot \sqrt{C_{H_{2,S}}} \quad (16)$$

Where, $k'_o = k' \cdot K_R \cdot \sqrt{K_H} \cdot C_{M1} \cdot C_{M2}^2$

M1, M2 = Catalyst active sites

Despite the reaction rate law that is described in equation 16, we have assumed a 1st order reaction with respect to the surface concentration of hydrogen, $C_{H_{2,S}}$, and zero order with respect to the surface concentration of unsaturated organic compound, $C_{R-CH=CH_{2,S}}$. In order to take into account the reaction rate law which is described in equation 16, we need to introduce an appropriate expression of the observed reaction constant of the surface reaction, k'_{obs}.

- $V_L \cdot MTR_{H_2,4} = \varepsilon \cdot k'_{obs} \cdot W_c \cdot C_{H_2,S}$
- $-W_c \cdot R'_{H_2} = W_c \cdot \varepsilon \cdot k'_o \cdot C_{R-CH=CH_{2,S}} \cdot \sqrt{C_{H_{2,S}}}$
- $V_L \cdot MTR_{H_2,4} = -W_c \cdot R'_{H_2}$

$$k'_{obs} = k'_o \cdot C_{R-CH=CH_{2,S}} \cdot \frac{1}{\sqrt{C_{H_{2,S}}}}$$

We substitute $C_{H_{2,S}}$ from equation 12,

$$k'_{obs} = k'_o \cdot C_{R-CH=CH_{2,S}} \cdot \frac{1}{\sqrt{\beta \cdot C_{H_2,i}}} \quad (17)$$

Substituting the expression of k'_{obs} to equation 8 and rearranging, we conclude to the following equation which describes the overall mass transfer resistance of the hydrogenation process, $\Omega_{H_2,tot}$.

$$\frac{C_{H_2,i}}{MTR_{H_2}} = \frac{1}{K_L \cdot \alpha} + \frac{1}{K_S \cdot \alpha_S \cdot \frac{W_c}{V_L}} + \frac{1}{\varepsilon \cdot k'_o \cdot C_{R-CH=CH_{2,S}} \cdot \frac{1}{\sqrt{\beta \cdot C_{H_2,i}}} \cdot \frac{W_c}{V_L}} \quad (18)$$

We substitute the expression of k'_{obs} to $\Omega_{H_2,R}$ and we rewrite the expression of factor β.

$$\beta = \frac{\Omega_{H_2,R}}{\Omega_{H_2,tot}} = \frac{\frac{1}{\varepsilon \cdot k'_o \cdot C_{R-CH=CH_{2,S}} \cdot \frac{1}{\sqrt{\beta \cdot C_{H_2,i}}} \cdot \frac{W_c}{V_L}}}{\Omega_{H_2,tot}}$$

$$\sqrt{\beta} = \frac{\frac{1}{\varepsilon \cdot k'_o \cdot C_{R-CH=CH_{2,S}} \cdot \frac{W_c}{V_L}} \cdot \sqrt{C_{H_2,i}}}{\Omega_{H_2,tot}} \quad (19)$$

Table 1 gives the definition of each of the resistances. Table 2 illustrates which of the terms of equation 18 change with respect to the process variables (N, $C_{H_2,i}$, T) and catalyst concentration.

Methods

Materials

Methanol 99.9%, styrene 99%, decane 99%, which were purchased from Sigma Aldrich, were used as solvent, substrate and internal standard, respectively. Compressed pure hydrogen (UN: 1049) was purchased from BOC. 5% Palladium on activated carbon (Type 87L) was purchased from Johnson Matthey.

Hydrogenation of styrene

We chose the hydrogenation of styrene as case study to illustrate the suggested methodology. Experiments were performed in a 0.6 L batch stirred autoclave reactor (Parr Instrument Company, USA), equipped with two 45^o pitched turbine type impellers. The diameter of the vessel is 6.5 cm and the diameter of the impellers is 3.5 cm. One impeller was located near the bottom and the second impeller positioned near the surface of the liquid to pull reactant gas down to the liquid phase. The reactor was used in continuous flow with respect to hydrogen. Reaction was monitored by measuring the consumption of hydrogen using a mass flow controller in the inlet of the reactor. Figure 13 illustrates typical accumulative consumption curves of hydrogen in several agitation speeds. The mass flow controller was set to keep the reactor pressure constant. Pressure transducer is used to monitor pressure. The temperature of reaction mixture is maintained at the desired value by using an automatic temperature control. Figure 4 illustrates the experimental set-up.

Table 3 gives the operating conditions of the reactor and Table 4 summaries the design characteristics of the reactor. The ratio between liquid and gas phase, V_L/ V_G, was about 1/2.

Results and Discussion

Separation of mass transfer resistances

Separation of $\Omega_{H_2,i-L}$ from $\Omega_{H_2,L-S}$ and $\Omega_{H_2,R}$

The initial mass transfer rate is independent of styrene concentration. We rewrite equation (18) as below,

$$\frac{\mathrm{C_{H_2,i}}}{\mathrm{MTR_{H_2}}} = \frac{1}{\mathrm{K_L \cdot \alpha}} + \left(\frac{1}{\mathrm{K_S \cdot \alpha_S}} + \frac{1}{\varepsilon \cdot \mathrm{k'_o} \cdot \frac{1}{\sqrt{\beta \cdot \mathrm{C_{H_2,i}}}}} \right) \cdot \frac{\mathrm{V_L}}{\mathrm{W_c}} \qquad (20)$$

If one observes the initial $\mathrm{MTR_{H_2}}$ at different catalyst loading, $\mathrm{W_c}$, keeping same the rest of the variables (N, $\mathrm{C_{H_2,i}}$ and T) and plots $\Omega_{H_2,tot}$ vs $\mathrm{V_L/W_c}$, then the intercept of the graph will be equal to the $1/\mathrm{K_L\alpha}$. Repeating the same procedure at different agitation speed, the $1/\mathrm{K_L\alpha}$ can be calculated for several agitation speeds. Figure 5 illustrates the results. Each subgraph corresponds to a set of different experiments under the same stirrer speed. In each subgraph, the reaction temperature and the concentration of hydrogen in gas-liquid interface are kept constant.

The catalyst concentrations varied from 0.05 g cat/L solvent to 1.5 g cat/L solvent while each experiment was repeated three times. The correlation coefficient, r, was calculated in order to measure the linear association between the experimental data of $\Omega_{H_2,tot}$ and $\mathrm{V_L/W_c}$ at each agitation speed. To check if the linear regression models fit the data, the coefficient of determination, r^2, was calculated. The model residuals analysis

showed lack of any particular pattern. The confidence intervals for the models' parameters were also calculated and they are presented in Table 4. Figure 8 summarise the results. The most significant effect of agitation speed on $\Omega_{H_2,\mathrm{i-L}}$ of agitation speed was observed between 200 and 500 rpm. From 500 rpm up to 900 rpm the agitation speed affects $\Omega_{H_2,i-L}$ less. Taking into account the 95% confidence intervals of the calculated parameters, a plateau is developed at agitation speed higher than 800 rpm. The plateau could have been reached because of impeller overloading that affects its ability to disperse all the gas supplied.

Separation of $\Omega_{H_2,R}$ from $\Omega_{H_2,i-L}$ and $\Omega_{H_2,L-S}$

We rewrite equation (18) as below,

$$\frac{\mathrm{C_{H_2,i}}}{\mathrm{MTR_{H_2}}} = \frac{1}{\mathrm{K_L}\cdot\alpha} + \frac{1}{\mathrm{K_S}\cdot\alpha_S\cdot\frac{\mathrm{W_c}}{\mathrm{V_L}}} + \frac{1}{\varepsilon\cdot k_o'\cdot\beta^{-0.5}\cdot\frac{\mathrm{W_c}}{\mathrm{V_L}}}\cdot \mathrm{C_{H_2,i}^{0.5}} \quad (21)$$

By changing the hydrogen pressure in the reactor vessel, one is able to manipulate the concentration of hydrogen in gas-liquid interface. We conducted experiments at several hydrogen pressures observing the initial $\mathrm{MTR_{H_2}}$. Each experiment took place under same a) stirrer speed, b) temperature and c) catalyst concentration. It should be noticed that the experiments took place under conditions where $\Omega_{H_2,R} > \Omega_{H_2,i-L}$ and $\Omega_{H_2,R} > \Omega_{H_2,L-S}$. This is because we need the chemical reaction to be the limiting regime. Otherwise gas to liquid or liquid to solid mass transfer is the limiting regime of the process, resulting in the $\Omega_{H_2,tot}$ independence of $\sqrt{\mathrm{C_{H_2,i}}}$. This independence does not allow us to calculate the factor of $\sqrt{\mathrm{C_{H_2,i}}}$ in equation 21.

We calculated the total mass transfer resistance ($\Omega_{H_2,tot} = \mathrm{C_{H_2,i}}/\mathrm{MTR_{H_2}}$) at each hydrogen concentration. The plot of $\Omega_{H_2,tot}$ with respect to $\mathrm{C_{H_2,i}^{0.5}}$ is distinguished in two different regions (Figure 6a). Both regions have constant slopes, one higher than the other and constant intercepts. This indicates that the factor of $\mathrm{C_{H_2,i}^{0.5}}$ and the external mass transfer resistances are constant in the range of each region. Therefore, one is able to calculate the $\Omega_{H_2,R}/\mathrm{C_{H_2,i}^{0.5}}$ term by applying linear regression in the data of each region.

The experiments took place using one type of impellers (two 45^{o} pitched turbine type impellers) and one experimental set-up which is shown in figure 4 and its details are given in table 4. Therefore, we cannot extract conclusions if the two-region behaviour is case specific or not.

Once the $\Omega_{H_2,R}/\mathrm{C_{H_2,i}^{0.5}}$ term has been calculated, the $\Omega_{H_2,R}$ at 0.2 MPa, 1200rpm and 0.05 g catalyst/ L solvent is calculated. Given the calculated $\Omega_{H_2,R}$ and the value of $\Omega_{H_2,tot}$ under the same conditions (0.2 MPa, 1200rpm and 0.05 g catalyst/ L solvent), the factor β is calculated.

From values of the factor β and the $\Omega_{H_2,R}$ at 0.2 MPa, 1200rpm and 0.05 g catalyst/ L solvent, the term $\sqrt{\mathrm{C_{H_2,i}}}/\varepsilon \cdot \mathrm{k}_o'$ is calculated. We have already noticed that the term $\sqrt{\mathrm{C_{H_2,i}}}/\varepsilon \cdot \mathrm{k}_o'$ is independent of agitation speed. The factor β depends on agitation speed, resulting in $\Omega_{H_2,R}$ dependence on agitation speed. Using equation 19 and the value of the term $\sqrt{\mathrm{C_{H_2,i}}}/\varepsilon \cdot \mathrm{k}_o'$ the square root of factor β is calculated at agitation speeds from 200-1200 rpm and in given catalyst concentration. Once we have got the factor β at any agitation speed, we are able to calculate $\Omega_{H_2,R}$ at any agitation speed. The resistance of liquid-solid interface, $\Omega_{H_2,L-S}$ is calculated for that particular pressure range by subtracting

$\Omega_{H_2,i-L}$ and $\Omega_{H_2,R}$ from $\Omega_{H_2,tot}$. Figure 9 illustrates the steps of the procedure of calculations.

In this point, we need to notice that if the process is limited by the surface chemical reaction, the slope of $\Omega_{H_2,tot}$ vs $\sqrt{\mathrm{C_{H_2,i}}}$ should be non-zero. Otherwise gas to liquid or liquid to solid mass transfer is the limiting regime of the process. Figure 6b illustrates this fact, at 1200 rpm and 0.05 g catalyst/ L solvent (case 1), $\Omega_{H_2,tot}$ depends on square root of hydrogen concentration. On the other hand, at 900 rpm and 0.125 g catalyst/ L solvent (case 2), $\Omega_{H_2,tot}$ is independent of hydrogen concentration. Figure 7 illustrates the contribution of each individual mass transfer resistances for the case 1 and 2.

The decreasing slope of the plot of $\Omega_{H_2,tot}$ with respect to $\mathrm{C_{H_2,i}^{0.5}}$ indicates that the factor β also decreasing. This means that the external mass transfer resistance increases from region 1 to region 2. This is also obvious from the increased intercept. Taking into account that the density and surface tension of the liquid phase are practically constant between 0.3-1.1 MPa, the gas-liquid mass transfer coefficient can be considered constant[2]. The increase of external mass transfer resistance may be caused by changes of the hydrodynamics patterns due to the increase of pressure.

Figure 8 summarises the separated mass transfer resistances with respect to agitation speed. $\Omega_{H_2,L-S}$ presents the most significant decrease between 300 and 400 rpm indicating that the suspension speed lies on that range. A bump of $\Omega_{H_2,L-S}$ takes place between 700 and 900 rpm. This may happen because at 700 rpm the stirrer starts pumping large gas volumes which make the density of the gas-liquid mixture to decrease and to cause the formation of gas cavities behind the stirrer blades. This decrease of density and the formation of gas cavities lead to a decrease of the power input with respect to the power

input into a pure liquid at the same agitation speed[26-29]. In other words, the gassed system needs higher agitation speed in order to have the same power input as the ungassed. Apart from the bump, the $\Omega_{H_2,L-S}$shows the same trend as $\Omega_{H_2,i-L}$, reaching a plateau.

Consequently, the mass transfer resistances are independent of agitation speed after a critical value of agitation speed. Therefore, the limiting regime of fast three-phase reactions cannot be ensured just by observing the plateau of mass transfer rate against agitation speed plots. This is because the plateau can be due to either the external mass transfer resistances or chemical reaction rate. On the other hand, the chemical reaction rate regime is ensured if we calculate each resistance and we ascertain that the highest resistance is $\Omega_{H_2,R}$.

Correlations

Gas-liquid mass transfer coefficient, $K_L \cdot \alpha$

Several correlations have been developed for the calculation of the gas-liquid mass transfer coefficient. We used the classical correlation based on the theory of isotropic turbulence using the power consumption per liquid volume and the superficial gas velocity to compare our experimental data[27, 30-35].

$$\mathrm{K_L} \cdot \alpha = B_1 \cdot \left(\frac{P}{V_L}\right)^{a_1} \cdot u_{sg}^{b_1} \quad (22)$$

The power consumption in an ungassed vessel is correlated by using the power number, N_p, and the impeller Reynolds number, Re_{im}[27, 36].

$$\mathrm{N}_P = \frac{P}{\rho_L \cdot N^3 \cdot D_{im}^5} \quad (23)$$

Once the impeller Reynolds number has been calculated the power number is approximated by using appropriate graphs of N_p with respect to $Re_{im.}$ We used the graph which is developed by Bates et al. [37]. In the case of 45° pitched turbine type impellers the power number is constant for impeller Reynolds number higher than 10^3. The impeller Reynolds number of our system is ranged from 6405 to 38433, so we considered the power number constant for our application. The power number when more than one impellers are used can be approximated as the power number of single impeller multiplied by the number of impellers ($\mathrm{N}_{P,n} = n \cdot \mathrm{N}_{P,1}$)[38].

Rearranging equation 23 with respect to power consumption and dividing by the liquid volume V_L, we conclude to equation 24.

$$\frac{P}{V_L} = \frac{n \cdot \mathrm{N}_{P,1} \cdot \rho_L \cdot D_{im}^5}{V_L} \cdot N^3 \quad (24)$$

Using the same vessel and configuration of stirrers, the same volume of liquid and under conditions which ensure constant density of liquid phase the $n \cdot \mathrm{N}_{P,1} \cdot \rho_L \cdot D_{im}^5 / V_L$ term can be considered constant.

During the experiments the superficial velocity of hydrogen was being determined by the consumption rate of hydrogen because of the chemical reaction. We plotted the superficial velocity of the hydrogen against the agitation speed. From Figure 10 one realises that the superficial velocity of hydrogen is practically constant.

Substituting equation 24 to equation 22 and taking into account that the superficial velocity of hydrogen is constant,

$$\mathrm{K_L} \cdot \alpha = B \cdot N^{3 \cdot a_1} \quad (25)$$

$$\frac{1}{\mathrm{K_L} \cdot \alpha} = \frac{1}{B} \cdot N^{-3 \cdot a_1} \quad (26)$$

Where, $B = B_1 \cdot u_{sg}^{b_1} \cdot \left(n \cdot \mathrm{N}_{P,1} \cdot \rho_L \cdot D_{im}^5 / V_L\right)^{a_1}$

By applying nonlinear regression analysis, the exponent a_1 and the constant term B were approximated. Figure 11 summarises the results. The exponent a_1 which is calculated from our data is equal to 0.47. Several researchers have reported the exponent a_1 for their systems to be between 0.3-0.65, see Table 6. This means that the behaviour of our system, with respect to $\mathrm{K_L} \cdot \alpha$, is in agreement with the results presented in the literature, justifying the way which we used in order to calculate the $\mathrm{K_L} \cdot \alpha$.

Liquid-solid mass transfer coefficient, $K_S \cdot \alpha_S$

In the case of liquid-solid mass transfer coefficient we used the well-known equation which correlates the Sherwood number with Reynolds and Schmidt number for forced-convection mass transfer from single spheres[39, 40].

$$Sh = 2 + A \cdot \left(Re_p\right)^m \cdot Sc^n \quad (27)$$

To calculate the Reynolds number an appropriate expression of velocity is required. That expression is given from Kolmogoroff's theory of isotropic turbulence which suggests

that the turbulent velocities are a function of only a) the rate of energy dissipation and b) the kinematic viscosity of the fluid[41].

The Reynolds number of particle, Re_p, is defined as,

$$Re_p = \epsilon \cdot \frac{d_p^4}{v_L^3} = \epsilon \cdot \frac{d_p^4 \cdot \rho_L^3}{\mu_L^3} \quad (28)$$

The average energy dissipation rate per mass unit in the stirred tank is given by the equation 29[27].

$$\epsilon \approx \epsilon_{aver} = \frac{P}{\rho_L \cdot (\pi/4) \cdot D_{im}^2 \cdot H} \quad (29)$$

Substituting the expression of power input, P, to equation 29,

$$\epsilon \approx \epsilon_{aver} = \frac{n \cdot \mathrm{N}_{P,1} \cdot \rho_L \cdot D_{im}^5}{\rho_L \cdot (\pi/4) \cdot D_{im}^2 \cdot H} \cdot N^3 \quad (30)$$

Therefore, the Reynolds number of particle, Re_p, is expressed as,

$$Re_p = \epsilon \cdot \frac{d_p^4 \cdot \rho_L^3}{\mu_L^3} = \frac{n \cdot \mathrm{N}_{P,1} \cdot D_{im}^3}{(\pi/4) \cdot H} \cdot \frac{d_p^4 \cdot \rho_L^3}{\mu_L^3} \cdot N^3 \quad (31)$$

To approximate the exponent of particle Reynolds number, we set the Schmidt number exponent to 1/3 as this is the most frequent value in the literature[42].

We have already mentioned that the gassed system needs higher agitation speed in order to have the same power input as the ungassed. Our reactor system can be considered as ungassed up to 600 rpm and gassed for agitation speeds higher than 600 rpm. If one

observes the $\Omega_{H_2,L-S}$ vs N, it is clear that the $\Omega_{H_2,L-S}$ at 600 rpm and 1000 rpm is almost the same. Because of that, we assumed that the power input at 600 rpm and 1000 rpm is the same. In other words, we assumed that the higher agitation speed has compensated the effect of gassing. Therefore, we did not take into account the interval from 700 rpm to 900 rpm at the correlations.

By applying nonlinear regression analysis to $(Sh-2)/Sc^{1/3}$ vs Re_p, the exponent m and the constant term A were approximated. Figure 12 summarises the results. The exponent m which calculated from our data is equal to 0.46. That value agrees well with the classical Fr$\ddot{o}$ssling equation[12, 43, 44] in which the exponent of particle Reynolds number is 1/2. Gholap et al. [10] and Teshima and Ohashi [39] have reported a lower exponent of particle Reynolds number equal to 0.41 while Sano et al. [45] reported an exponent of particle Reynolds number equal to 0.25 for agitated vessels and bubble columns. In our system the constant term A equals 1.86. In the case of steady state diffusion in a stagnant fluid, the Sherwood number equals 2. The term A indicates the contribution of the forced convection to the mass transfer. High values of A indicates high contribution of forced convection to the mass transfer. Miller [46] has reported the A equals 1.1 for mass transfer from fixed solid spheres in agitated vessels. This is in agreement with our results if one thinks that the contribution of forced convection in a system of free moved spheres should be higher than the contribution of fixed spheres. This means that the behaviour of our system, with respect to $K_S \cdot \alpha_S$, is in agreement with the results presented in the literature, justifying the way which we used in order to calculate the $K_S \cdot \alpha_S$.

Conclusion

The mass transfer resistances in a three-phase mechanically agitated slurry reactor can be calculated by changing catalyst loading and manipulating only the agitation speed and the pressure of hydrogen. This allows to avoid the use of different catalyst particles and give the chance to calculate the mass transfer resistances without caring about the type of catalyst. The plateau at mass transfer rate against agitation speed plots is not enough to ensure that the process is limited by either chemical reaction or external resistances. On the other hand, the limiting regime is ensured by the highest resistance. Our method to determine the limiting regime can be used even if none of the mass transfer rates can be neglected. To justify the proposed methodology by comparing our results with those in the literature, we developed correlations of $K_L \cdot \alpha$ and $K_S \cdot \alpha_S$. The developed correlations are in agreement with the literature. Additional work is needed in order to clarify the effects of pressure on external mass transfer resistances, especially on liquid-solid mass transfer resistance.

Acknowledgments

The generous support by Syngenta, EPSRC funding and the University of Leeds is acknowledged.

Notation

B, B_1	constant terms in Eqs. 22, 25 and 26
b_1	exponent of superficial gas velocity in Eq. 22
$C_{H_2,i}$	concentration of hydrogen in gas-liquid interface, $[\mathrm{kmol/m^3 liquid}]$

$C_{H_2,L}$ concentration of hydrogen in liquid phase,[$\mathrm{kmol/m^3 liquid}$]

$C_{H_2,S}$ concentration of hydrogen at catalyst surface, [$\mathrm{kmol/m^3 liquid}$]

$C_{R-CH=CH_2,L}$ concentration of unsaturated organic compound at catalyst surface,

[$\mathrm{kmol/m^3 liquid}$]

$C_{R-CH=CH_2,L}$ concentration of unsaturated organic compound in liquid phase,

[$\mathrm{kmol/m^3 liquid}$]

C_{H-M1} concentration of adsorbed hydrogen at the active sites of catalyst per area of catalyst, [$\mathrm{kmol/m^2 catalyst}$]

C_{M1}, C_{M2} concentration of active sites of catalyst per area of catalyst, [$\mathrm{kmol/m^2 catalyst}$]

C_P concentration of adsorbed unsaturated organic compound at the active sites of catalyst per area of catalyst, [$\mathrm{kmol/m^2 catalyst}$]

D_{im}, D_R diameter of impeller and reactor, [m]

$\mathfrak{D}$ diffusion coefficient, [$\mathrm{m^2/min}$]

d_p diameter of particle, [m]

H blade height of impeller, [m]

H_E Henry constant,[$\mathrm{Pa \cdot m^3/kmol}$]

K_G gas-liquid mass transfer coefficient related to gas side film,[$\mathrm{kmol/Pa \cdot min \cdot m^2}$]

K_L gas-liquid mass transfer coefficient related to liquid side film, [$\mathrm{m/min}$]

K_S liquid-solid mass transfer coefficient, [$\mathrm{m/min}$]

K_H, K_R chemisorption equilibrium constants,[$\mathrm{m^3 liquid/kmol\ compound}$]

k'_{obs} observed rate constant for 1st order reaction based on unit catalyst mass, [$\mathrm{m^3 liquid/kg\ catalyst \cdot min}$]

k'_o corrected observed rate constant for 1st order reaction based on unit catalyst mass,

[$\mathrm{(m^3 liquid)^2 \cdot\ (kmol\ H_2)^{0.5}/kg\ catalyst \cdot min \cdot (m^3 liquid)^{0.5} \cdot (kmol\ R-CH=CH_2)}$]

MTR mass transfer rate, [$\mathrm{kmol/m^3 liquid \cdot min}$]

N stirrer speed, [rpm]

N_P power number

n	number of impellers
P_{H_2}	pressure of Hydrogen, Pa
P	power input, [J/min]
$Re_{im} = \frac{\rho_L \cdot N \cdot D_{im}^2}{\mu_L}$	Reynolds number of impeller, [-]
$Re_p = \frac{\epsilon \cdot d_p^4 \cdot \rho_L^3}{\mu_L^3}$	Reynolds number of particle, [-]
R'_{H_2}	reaction rate based on unit catalyst mass, [$\mathrm{kmol\ H_2/\ kg\ catalyst \cdot min}$]
r, r^2	correlation coefficient, coefficient of determination, respectively
$Sc = \frac{\mu_L}{\mathfrak{D} \cdot \rho_L}$	Schmidt number
$Sh = \frac{K_S \cdot d_p}{\mathfrak{D}}$	Sherwood number
T	temperature, [K]
u_{sg}	superficial gas velocity, [m/min]
V_G, V_L	volume of gas phase and liquid phase in the reactor, [m^3]
v_L	kinematic viscosity of liquid phase, [m^2/s]

W_C	mass of catalyst, [kg]

Greek letters

α	gas-liquid surface area, $\mathrm{m}^2/\mathrm{m}^3$ of liquid
α_s	area of catalyst per weight of catalyst, m^2/kg catalyst
α_1	exponent of power input per volume of liquid in Eq. 22
β	Vita factor
ε	effectiveness factor
ϵ	energy dissipation rate, [J $\cdot min^{-1}kg^{-1}$]
μ_L	dynamic viscosity, [kg$\cdot m^{-1}s^{-1}$
ρ_L, ρ_p	density of liquid phase and solid particle, [kg/m^3]
$\Omega_{H_2\mathrm{tot}}$, $\Omega_{H_2,\mathrm{i-L}}$, $\Omega_{H_2,\mathrm{L-S}}$, $\Omega_{H_2,\mathrm{R}}$	mass transfer resistances,[min]
$\Omega'_{H_2,\mathrm{L-S}}$, $\Omega'_{H_2,\mathrm{R}}$	mass transfer resistances based on catalyst concentration, [min $\cdot$ kg catalyst/m^3liquid]

Subscripts

i	gas-liquid interface

G	gas phase
L	liquid phase
S	solid phase

Literature Cited

1. Beenackers AACM, Swaau WPMV. Mass transfer in gas-liquid slurry reactors. Chemical Engineering Science. 1993;48:3109-3139.
2. Dietrich E, Mathieu C, Delmas H, Jenck J. Raney - nickel catalyzed hydrodynamics: Gas-liquid mass transfer in gas-induced stirred slurry reactors. Chemical Engineering Science. 1992;47:3597-3604.
3. Vernuccio S, Von Rohr PR, Medlock J. General kinetic modeling of the selective hydrogenation of 2-methyl-3-butyn-2-ol over a commercial palladium-based catalyst. Industrial & Engineering Chemistry Research. 2015;54:11543-11551.
4. Betti C, Badano J, Lederhos C, Maccarrone M, Carrara N, Coloma-Pascual F, Quiroga M, Vera C. Kinetic study of the selective hydrogenation of styrene over a pd egg-shell composite catalyst. Reaction Kinetics, Mechanisms and Catalysis. 2015;117:283-306.
5. Tiwari MS, Yadav GD, Ng FTT. Selective hydrogenation of 3,4-dimethoxybenzophenone in liquid phase over pd/c catalyst in a slurry reactor. Can. J. Chem. Eng. 2014;92:2157-2165.

6. Joshi AM, MacFarlane KS, James BR. Kinetics and mechanism of h2-hydrogenation of styrene catalysed by [rucl(dppb)(m-cl)]2 (dppb=1,4-bis(diphenylphosphino) butane). Evidence for hydrogen transfer from a dinuclear molecular hydrogen species. J. Organometallic Chem. 1995;488:161-167.

7. Hoffer BW, Schoenmakers PHJ, Mooijman PRM, Hamminga GM, Berger RJ, van Langeveld AD, Moulijn JA. Mass transfer and kinetics of the three-phase hydrogenation of a dinitrile over a raney-type nickel catalyst. Chemical Engineering Science. 2004;59:259-269.

8. Deimling A, Karandikar BM, Shah YT, Carr NL. Solubility and mass transfer of co and h2 in fischer-tropsch liquids and slurries. The Chemical Engineering Journal. 1984;29:127-140.

9. Cordova WA, Harriott P. Mass transfer resistances in the palladium catalysed hydrogenation of methyl linoleate. Chemical Engineering Science. 1975;30:6.

10. Gholap RV, Kolhe DS, Chaudhari RV, Emig G, Hofmann H. A new approach for the determination of liquid-solid mass-transfer coeffiecient in multiphase reactors. Chemical Engineering Science. 1987;42:1689-1693.

11. Ruether JA, Puri PS. Mass transfer effects in hydrogenations in slurry reactors. Can. J. Chem. Eng. 1973;51:345-352.

12. Levenspiel O. Chemical reaction engineering (3rd edition). New York: John Wiley & Sons, 1999.

13. Perego C, Peratello S. Experimental methods in catalytic kinetics. Catalysis Today. 1999;52:13.

14. Murthy AKS. Design and scale up of slurry hydrogenation systems. Chem Eng - New York. 1999;106:94-107.

15. Biardi G, Baldi G. Three-phase catalytic reactors. Catalysis Today. 1999;52:223-234.

16. Satterfield CN. Mass transfer in heterogeneous catalysis. Cambridge: M.I.T Press, 1970.

17. Herskowitz M, Smith JM. Trickle bed reactors: A review. AIChE Journal. 1983;29:18.

18. Liu Q, Takemura F, Yabe A. Solubility of hydrogen in liquid methanol and methyl formate at 20 to 140 celcius. J. Chem. Eng. Data. 1996;41:1141-1143.

19. Boudart M, G.Djega-Mariadassou. Kinetics of heterogeneous catalytic reactions. New Jersey: Princeton University Press, 1984.

20. Davis ME, Davis RJ. Fundamentals of chemical reaction engineering. New York: Mc Graw Hill, 2003.

21. Yu W-Y, Mullen GM, Mullins CB. Hydrogen adsorption and absorption with pd–au bimetallic surfaces. The Journal of Physical Chemistry C. 2013;117:19535-19543.

22. Conrad H, Ertl G, Latta EE. Adsorption of hydrogen on palladium single crystal surface. Surface Science. 1974;41:435-446.

23. Behm RJ, Christmann K, Ertl G. Adsorption of hydrogen on pd(100). Surface Science. 1980;99:320-340.

24. Baber AE, Tierney HL, Lawton TJ, Sykes ECH. An atomic-scale view of palladium alloys and their ability to dissociate molecular hydrogen. ChemCatChem. 2011;3:607-614.

25. Okuyama H, Siga W, Takagi N, Nishijima M, Aruga T. Path and mechanism of hydrogen absorption at pd(100). Surface Science. 1998;401:344-354.

26. Westerterp KR, Dierendonck LLV, Kraa JAD. Interfacial areas in agitated gas-liquid contactors. Chemical Engineering Science. 1963;18:157-176.

27. Garcia-Ochoa F, Gomez E. Theoretical prediction of gas–liquid mass transfer coefficient, specific area and hold-up in sparged stirred tanks. Chemical Engineering Science. 2004;59:2489-2501.

28. Vasconcelos JMT, Orvalho SCP, A.M.A.F.Rodrigues, S.S.Alves. Effect of blade shape on the performance of six-bladed disk turbine impellers. Ind. Eng. Chem. Res. 2000;39:203-213.

29. F.Kudrewizki, P.Rade. Model of dissipation of mechanical energy in gassed stirred tanks. Chemical Engineering Science. 1986;41:2247-2252.

30. Markopoulos J, Christofi C, Katsinaris I. Mass transfer coefficients in mechanically agitated gas-liquid contactors. Chemical Engineering & Technology. 2007;30:829-834.

31. Labík L, Moucha T, Kordač M, Rejl FJ, Valenz L. Gas-liquid mass transfer rates and impeller power consumptions for industrial vessel design. Chemical Engineering & Technology. 2015;38:1646-1653.

32. Kapic A, Heindel TJ. Correlating gas-liquid mass transfer in a stirred-tank reactor. Chemical Engineering Research and Design. 2006;84:239-245.

33. Karimi A, Golbabaei F, Mehrnia MR, Neghad M, Mohammad K, Nikpey A, Pourmand MR. Oxygen mass transfer in a stirred tank bioreactor using different impeller configutions for enviromental purposes. Iranian Journal of Enviromental Health Sciences & Engineering. 2013;10.

34. Moucha T, Linek V, Prokopová E. Gas hold-up, mixing time and gas–liquid volumetric mass transfer coefficient of various multiple-impeller configurations: Rushton turbine, pitched blade and techmix impeller and their combinations. Chemical Engineering Science. 2003;58:1839-1846.

35. Figueiredo MMLD, Calderbank PH. The scale-up of aerated mixing vessels for specified oxygen dissolution rates. Chemical Engineering Science. 1979;34:1333-1338.

36. Hiraoka S, Kato Y, Tada Y, Ozaki N, Murakami Y, Lee YS. Power consumption and mixing time in an agitated vessel with double impeller. Chemical Engineering Research and Design. 2001;79:805-810.

37. Bates RL, Fondy PL, Corpstein RR. An examination of some geometric parameters of impeller power. I&EC Process Design and Development. 1963;2:310-314.

38. Nienow AW, Lilly MD. Power drawn by multiple impellers in sparged agitated vessels. Biotechnology and Bioengineering. 1979;21:2341-2345.

39. Teshima H, Ohashi Y. Particle to liquid mass transfer in a rotating catalyst basket reactor. Journal of Chemical Engineering of Japan. 1977;10:3.

40. Hughmark GA. Mass transfer for suspended solid particles in agitated liquids. Chemical Engineering Science. 1969;24:291-297.

41. Brian PLT, Hales HB, Sherwood TK. Transport of heat and mass between liquids and spherical particles in an agitated tank. AIChE Journal. 1969;15:727-733.

42. Skelland AHP. Diffusional mass transfer. New York: John Wiley & Sons, 1974.

43. Middleman S. Mass transfer from particles in agitated systems: Application of kolmogoroff theory. AIChE Journal. 1965;11:750-761.

44. Rousseau RW. Handbook of separation process technology. Chichester;New York;: Wiley, 1987.

45. Sano Y, Yamaguchi N, Adachi T. Mass transfer coefficients for suspended particles in agitated vessels and bubble columns. Journal of Chemical Engineering of Japan. 1974;7:255-261.

46. Miller DN. Scale-up of agitated vessels. Ind. Eng. Chem. Process Des. Develop. 1971;10:365-375.

47. Robinson CW, Wilke CR. Oxygen absorption in stired tanks: A correlation for ionic strength effects. Biotechnology and Bioengineering. 1973;15:755-782.

48. Linek V, Sinkule J, Benes P. Critical assessment of gassing-in methods for measuring kla in fermentors. Biotechnology and Bioengineering. 1990;38:323-330.

49. Linek V, Vacek V, Benes P. A critical review and experimental verification of the correct use of the dynamic method for the determination of oxygen transfer in aerated agitated vessels to water, electrolyte solutions and viscous liquids. Chem. Eng. J. 1987;34:11-34.

50. Chandrasekharan K, Calderbank PH. Further observations on the scale-up of aerated mixing vessels. Chemical Engineering Science. 1980;36:819-823.

51. Riet KV. Review of measuring methods and results in nonviscous gas-liquid mass transfer in stirred vessels. I&EC Process Design and Development. 1979;18:357-364.

52. Yawalkar AA, Heesink ABM, Versteeg GF, Pangarkar VG. Gas-liquid mass transfer coefficient in stirred tank reactors. Can. J. Chem. Eng. 2002;80:840-848.

53. R. V. Chaudhari RVG, G. Emig and H. Hofmann. Gas liquid mass trasfer in "dead end" autoclave reactors. Can. J. Chem. Eng. 1987;65:8.

54. Machadot JRS, W.B.Streett. Equation of state and thermodynamic properties of liquid methanol from 298 to 4879 kelvin and pressures to 1040 bar. J. Chem. Eng. Data. 1983;28:218-223.

55. Samardžić ZM. Kinetics and mass transfer in the hydrogenation of 2-((1-benzyl-1,2,3,6-tetrahydropyridin-4-yl)methylene)-5,6-dimethoxy-2,3-dihydroinden-1-one hydrochloride over pt/c catalyst. Chemical and Biochemical Engineering Quarterly Journal. 2015;28:437-445.

LIST TABLE CAPTIONS

Table 1. Mass Transfer Resistances

Table 2. Term Dependency on Process Variables and Catalyst Concentration

Table 3. Reactor Operating Conditions

Table 4. Summary of Reactor Design Characteristics

Table 5. Linear Regression Results of $\Omega_{H_2,R}$ against V_L/W_c in several Agitation Speeds and 95% Confidence Interval of Estimated Parameters

Table 6. Values of Exponent α_1 from different Workers

Table 7. Summary of Physical Properties of Liquid and Solid Phase

LIST OF FIGURE CAPTIONS

Figure 1. Hydrogen dissociative chemisorption.

Figure 2. Molecular chemisorption of unsaturated organic compound.

Figure 3. Surface chemical reaction.

Figure 4. Experimental set-up.

Figure 5. Mass transfer resistance against catalyst concentration reciprocal at several agitation speeds.

Figure 6. Mass transfer resistance against square root of hydrogen concentration in gas-liquid interface (left a, right b).

Figure 7. Mass transfer resistances at 900rpm, 0.125 g catalyst/ L solvent and at 1200rpm, 0.05 g catalyst/ L solvent.

Figure 8. Mass transfer resistances against agitation speed using 0.125 g catalyst/ L solvent.

Figure 9. Steps of calculation of $\Omega_{H_2,R}$ and $\Omega_{H_2,L\text{-}S}$.

Figure 10. Hydrogen superficial velocity against stirrer speed.

Figure 11. Summary of $K_L \cdot \alpha$ correlation results.

Figure 12. Summary of $K_S \cdot \alpha_S$ correlation results

Figure 13. Total consumption of hydrogen volume

Table 1: Mass transfer resistances

Description		Expression	Definition
External mass transfer resistances	Resistance of gas-liquid interface	$\Omega_{H_2,i-L}$	$\frac{1}{K_L \cdot \alpha}$
	Resistance of liquid-solid interface	$\Omega_{H_2,L-S}$	$\frac{1}{K_S \cdot \alpha_S \cdot \frac{W_c}{V_L}}$
Resistance of internal catalyst pore structure and surface chemical reaction		$\Omega_{H_2,R}$	$\frac{1}{\varepsilon \cdot k'_{obs} \cdot \frac{W_c}{V_L}}$

Table 2: Term dependency on process variables and catalyst concentration

	Hydrogen Concentration, $C_{H_2,i}$	Stirrer Speed, N	Catalyst Concentration, $\frac{W_c}{V_L}$	Temperature, T
$\Omega_{H_2,i-L}$	✗	✓	✗	✓
$\Omega_{H_2,L-S}$	✗	✓	✓	✓
$\Omega_{H_2,R}$	✓	✓	✓	✓
$\frac{1}{\varepsilon \cdot k'_o \cdot C_{R-CH=CH_{2,S}} \cdot \frac{1}{\sqrt{C_{H_2,i}}}}$	✓	✗	✗	✓
β	✓	✓	✓	✓

Table 3: Reactor operating conditions

Temperature T (^{o}C)	Pressure P (MPa gauge)	Agitation Speed N (rpm)
32	0.2-1.0	200-1200

Table 4: Summary of reactor design characteristics

Reactor characteristics	
Reactor diameter, $\boldsymbol{D_R}$ [m]	$6.5\cdot 10^{-2}$
Reactor volume, $\boldsymbol{D_R}$ [$\boldsymbol{m^3}$]	$2\cdot 10^{-4}$
Impeller diameter, $\boldsymbol{D_{im}}$ [m]	$3.5\cdot 10^{-2}$
Number of impeller blades	4
Height of the blade, H [m]	$8\cdot 10^{-3}$
Number of impellers	2
Impellers distances from the vessel bottom, [m]	$3\cdot 10^{-3}$ and $5.4\cdot 10^{-2}$

Table 5: Linear regression results of $\Omega_{H_2,R}$ against V_L/W_c in several agitation speeds and 95% confidence interval of estimated parameters.

			95% Confidence interval of estimated resistances	
N (rpm)	Intercept (min)	Slope (min· $g\ cat \cdot L\ sol^{-1}$)	Intercept (min)	Slope (min· $g\ cat \cdot L\ sol^{-1}$)
200	1.3581	0.0776	± 0.0277	±0.0098
300	0.9072	0.0717	± 0.0887	±0.0181
400	0.5581	0.0334	± 0.0081	±0.0033
500	0.2986	0.0265	± 0.0110	±0.0035
600	0.2635	0.0246	± 0.0173	±0.0075
700	0.2348	0.0356	± 0.0166	±0.0059
800	0.1566	0.0409	± 0.0207	±0.0031
900	0.1133	0.0436	± 0.0142	±0.0022
1000	0.1523	0.0255	± 0.0138	±0.0024
1200	0.1909	0.0218	± 0.0472	±0.0076

Table 6: Values of exponent α_1 proposed by different workers.

Reference	α_1
Robinson and Wilke [47]	0.40
Linek et al. [48]	0.65
Linek et al. [49]	0.59
Chandrasekharan and Calderbank [50]	0.56
Riet [51]	0.4
Karimi et al. [33]	0.6
Yawalkar et al. [52]	0.47 0.4 0.54
Figueiredo and Calderbank [35]	0.3 – 0.6
R. V. Chaudhari [53]	0.63

Table 7: Summary of physical properties of liquid and solid phase

Physical property	Value
CH_3OH density[54], ρ_L $[Kg/m^3]$ (P=0.3 Mpa to 1.1 Mpa)	776.9
CH_3OH dynamic viscosity, μ_L $[Kg/m \cdot s]$ (T=32^{o}C)	$4.98 \cdot 10^{-4}$
Diffusion coefficient of H_2 – CH_3OH system[55], $\mathfrak{D}$ [m^2/min]	$19.2 \cdot 10^{-8}$
Particle density, ρ_p $[Kg/m^3]$	2100
Particle diameter, d_p [m]	$20 \cdot 10^{-6}$

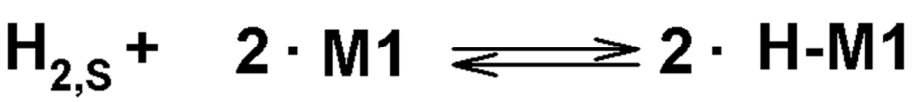

Hydrogen dissociative chemisorption
Figure 1
65x12mm (300 x 300 DPI)

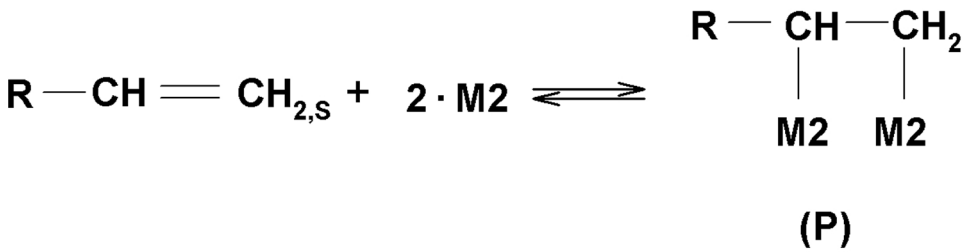

Molecular chemisorption of unsaturated organic compound
Figure 2
108x33mm (300 x 300 DPI)

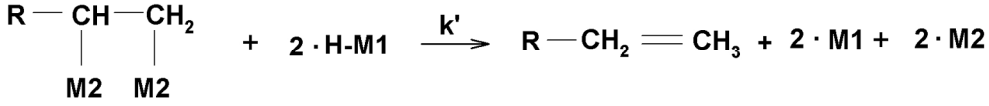

Surface chemical reaction
Figure 3
156x22mm (300 x 300 DPI)

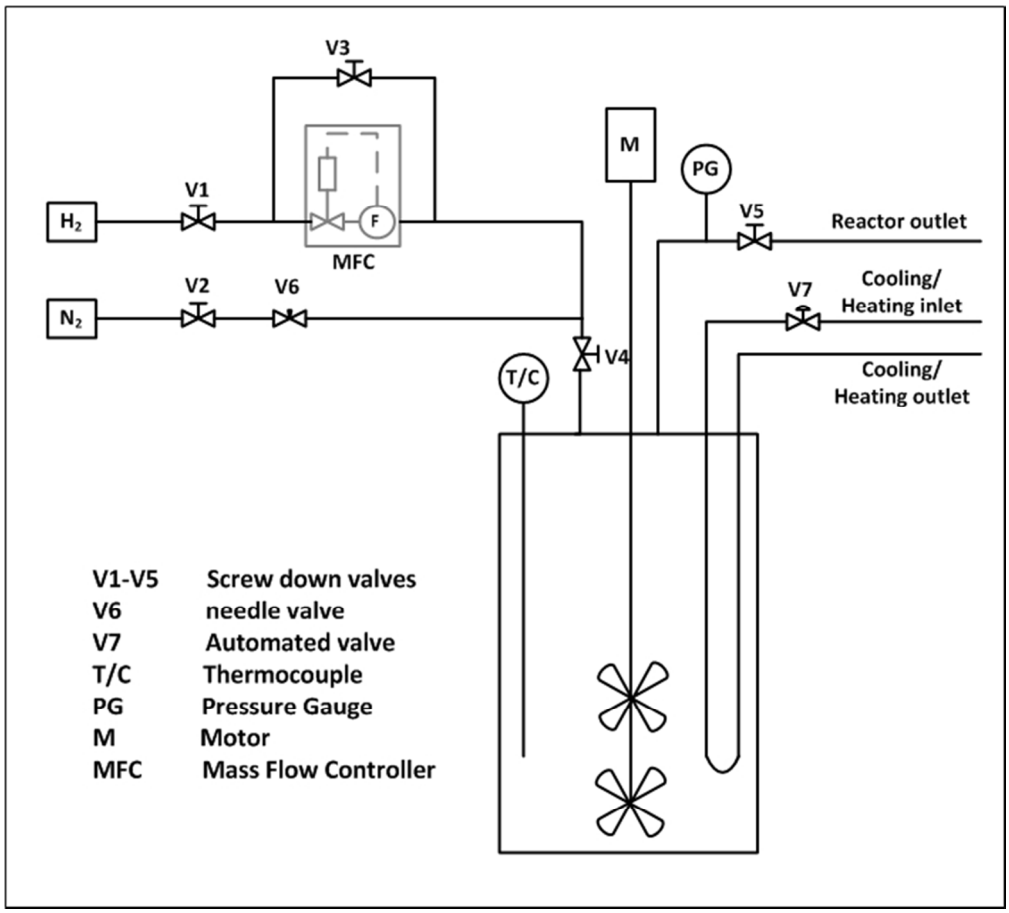

Experimental set-up
Figure 4
186x168mm (96 x 96 DPI)

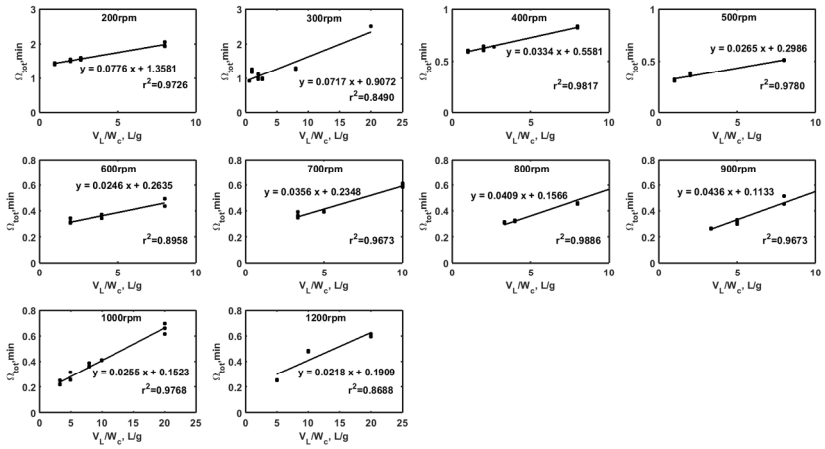

Mass transfer resistance against catalyst concentration reciprocal at several agitation speeds
Figure 5
508x255mm (96 x 96 DPI)

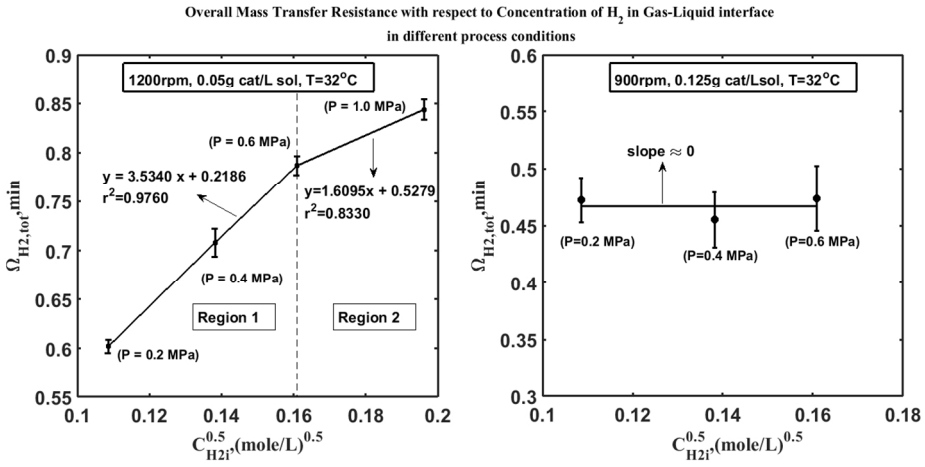

Mass transfer resistance against square root of hydrogen concentration in gas-liquid interface (left a, right b)

Figure 6

379x183mm (96 x 96 DPI)

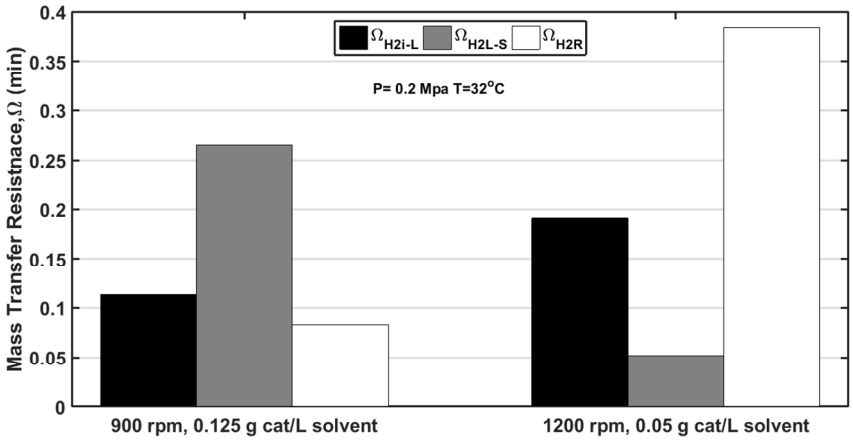

Mass transfer resistances at 900rpm, 0.125 g catalyst/ L solvent and at 1200rpm, 0.05 g catalyst/ L solvent
Figure 7
379x183mm (96 x 96 DPI)

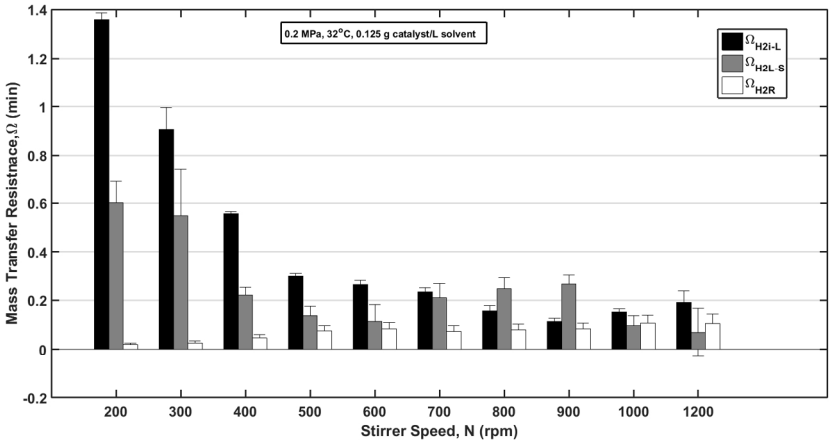

Mass transfer resistances against agitation speed using 0.125 g catalyst/ L solvent
Figure 8
508x242mm (96 x 96 DPI)

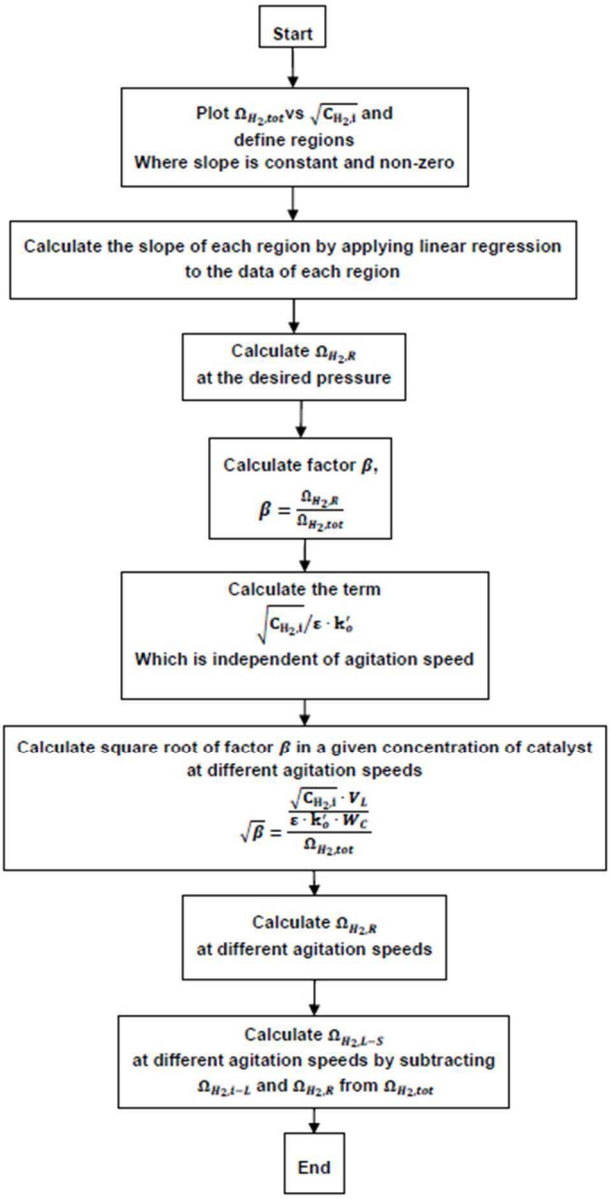

Figure_9_Steps_of_calculations
Figure 9
108x202mm (96 x 96 DPI)

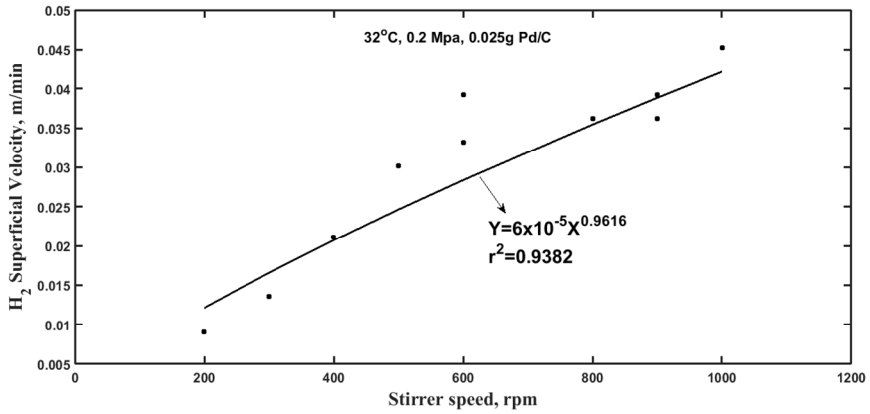

Hydrogen superficial velocity against stirrer speed
Figure 10
378x164mm (96 x 96 DPI)

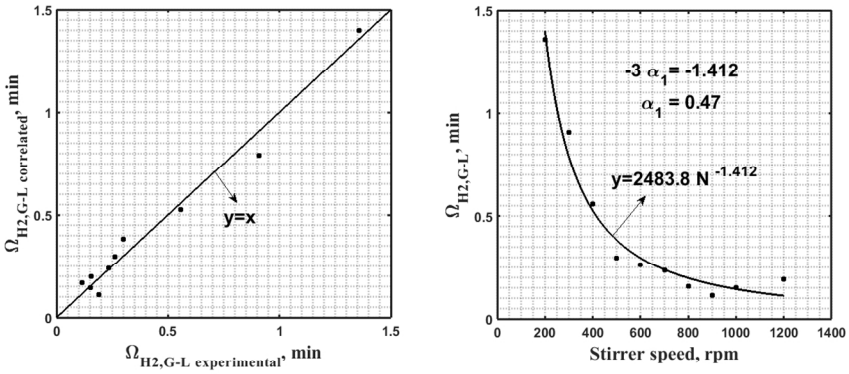

Summary of K_L·a correlation results
Figure 11
378x183mm (96 x 96 DPI)

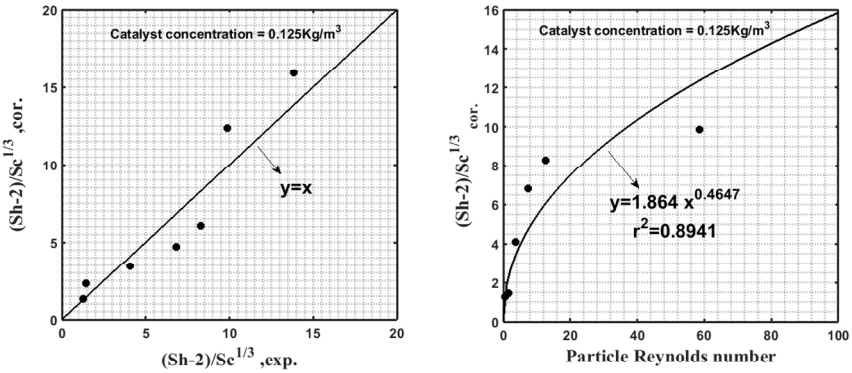

Summary of $K_S \cdot a_S$ correlation results
Figure 12
378x183mm (96 x 96 DPI)

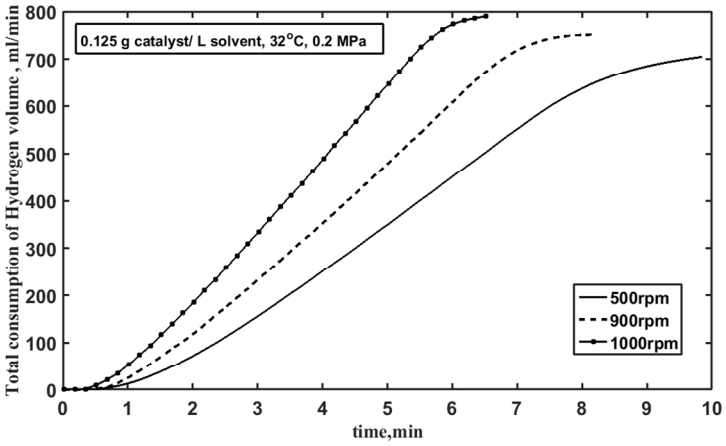

Total consumption of hydrogen volume
Figure 13
379x183mm (96 x 96 DPI)